A Proposal for Pentagonal Prism Spherical Hohlraum Experiments on OMEGA

W. Y. Wang and R. S. Craxton

Laboratory for Laser Energetics, University of Rochester

An important requirement for achieving ignition and gain through inertial confinement fusion is obtaining high levels of drive uniformity on a spherical capsule.[1–3] In the indirect-drive approach,[2] the fuel capsule is placed inside a case, known as a hohlraum, which is made of a high-Z material (typically gold) and converts the laser energy into an x-ray radiation field that provides a smooth drive on the capsule surface. On the National Ignition Facility (NIF),[4] the laser beams enter through two laser entrance holes (LEH's) on the axis of a cylindrical hohlraum.[2] For future laser systems, however, spherical hohlraums have attracted recent interest as a means of achieving better uniformity.[5–7] The work presented here explores the use of a spherical hohlraum, known as a pentagonal prism (PEPR) hohlraum, that will allow spherical hohlraums to be tested before future large-scale laser systems are constructed. The PEPR hohlraum has seven LEH's and is well suited to the OMEGA geometry. Proposed experiments on OMEGA are predicted to produce highly uniform compressions of the capsule.

The first spherical hohlraum to be proposed was the tetrahedral hohlraum,[8–10] shown in Fig. 1(a), with four LEH's located at the vertices of a tetrahedron. Tetrahedral hohlraum experiments were performed on OMEGA, producing highly uniform capsule compressions[11,12] consistent with the radiation drive on the capsule having less than 1% nonuniformity. Recently, octahedral hohlraums [Fig. 1(b)] were proposed as a more-uniform alternative to cylindrical and tetrahedral hohlraums, with flux nonuniformity as low as 0.1% (Refs. 5–7). The octahedral hohlraum has six LEH's corresponding to the centers of the faces of a cube or the vertices of an octahedron.

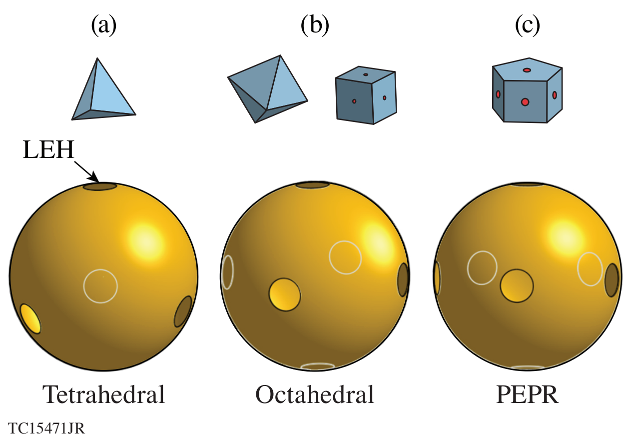

Figure 1
(a) Tetrahedral, (b) octahedral, and (c) pentagonal prism (PEPR) hohlraums. Laser entrance holes on the far side of the hohlraums are shown in outline.

Although the 60-beam OMEGA laser is geometrically unsuitable for driving octahedral hohlraums (as is also true of the NIF), the PEPR hohlraum [Fig. 1(c)] is well matched to the symmetry of the OMEGA target chamber, whose beam configuration has fivefold symmetry about the vertical axis. The LEH's of the PEPR hohlraum are based on the faces of a pentagonal prism, with five LEH's around the equator and one on each pole. This configuration was first suggested by Farmer *et al.*[13]

The PEPR hohlraum design presented here has dimensions taken from Ref. 10: the hohlraum diameter is 2800 μm, the capsule diameter is 550 μm, and the LEH diameter is 700 μm. Five beams enter each of the two polar LEH's and ten beams enter each of the equatorial LEH's. Figure 2(a) shows which beams enter each LEH. The angle of incidence θ_i relative to the LEH normal ranges from 21.4° (for beams passing through the polar LEH's) to 69.7°. For comparison, θ_i ranges from 23.2° to 58.8° for the OMEGA tetrahedral hohlraum[10] and from 21.2° to 52.4° for the NIF. The ray paths of the beams passing through the polar LEH's are shown in Fig. 2(b). They are focused inside the hohlraum to maximize the clearance from the capsule, as was done for the earlier tetrahedral hohlraum experiments on OMEGA. There are problems associated with the use of small angles of incidence on large systems such as the NIF, including laser–plasma instabilities along the large propagation distances and absorption in the hohlraum plasma. The proposed octahedral hohlraum avoids low values of θ_i because all beams enter in the optimal range of 50° to 60°.

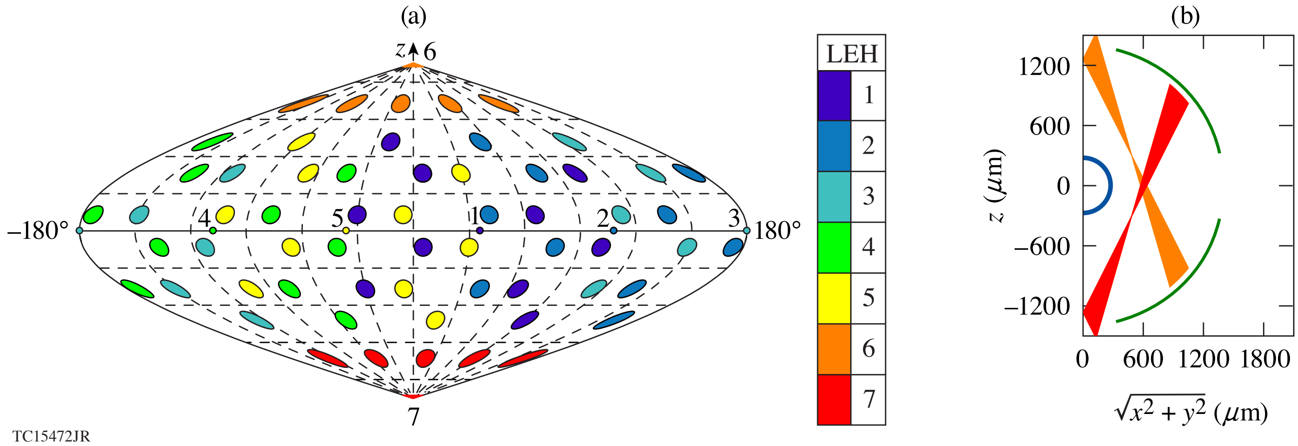

Figure 2
(a) LEH assignments used in *LORE* simulations for a PEPR hohlraum on OMEGA. Colors of beam ports represent LEH assignments. The small colored circles indicate the LEH locations. (b) Ray paths of beams entering through the LEH's (6 and 7) on the z axis. These beams are focused inside the hohlraum to maximize the clearance from the capsule.

The PEPR hohlraum is analyzed using a new view-factor code *LORE*,[14] which follows the physics model used in the code *BUTTERCUP*.[9] *LORE* traces beam paths starting from the target chamber port. Each beam is divided into multiple rays, each traveling through the best-focus point of the beam. *LORE* finds the intersection of each ray with the hohlraum wall and includes an *ad hoc* model of how much energy is deposited at that point and how much is reflected to the next intersection point. Typically, all the energy is deposited at the first intersection since the hohlraum wall is strongly absorbing. Figure 3(a) shows contours of deposited energy. One can see 60 distinct laser spots, spread fairly uniformly over the hohlraum wall. As recognized in Ref. 9, this is desirable for capsule uniformity. The beam spots are all clear of the LEH's.

After tracing all the beams, *LORE* determines a spatially independent background radiation temperature T_r by assuming a Planckian radiation field in the hohlraum. T_r is calculated by balancing the power entering the radiation field (the absorbed laser power multiplied by the laser-to-radiation conversion efficiency) with the power lost to the hohlraum wall, the capsule, and the LEH's. Of particular importance is the loss to the wall, equal to $\sigma T_r^4(1-\alpha_w)A_w$, where σ is the Stefan–Boltzmann constant, α_w is the wall albedo, and A_w is the wall area. Early in time, the albedo is low and most of the radiation incident on the wall goes into heating the wall. Later in time, the heated wall re-radiates most of its incident energy into the hohlraum and the albedo approaches unity.

Next, *LORE* calculates the emitted radiation flux at every point on the wall as the sum of the re-radiated portion of the incoming radiation $\left(\alpha_w \sigma T_r^4\right)$ and the portion of the absorbed laser flux that is converted to radiation. The emitted radiation flux I_e is parametrized in terms of the effective radiation temperature T_e, defined at each point on the wall such that $\left(I_e = \sigma T_e^4\right)$.

To determine the radiation uniformity on the capsule, *LORE* scans over multiple points on the capsule. For each point, *LORE* integrates the radiation flux I_e over all viewing directions. These integrals typically involve scanning over 60,000 points on the capsule and, for each point, looking along ~100,000 directions. A contour plot of the flux variations on the capsule is given in Fig. 3(b) for an albedo α_w of 0.85. The nonuniformity level is very low at 0.6% rms.

Figure 3(b) shows that, while the variations in drive on the capsule are very small, the strongest drive occurs at the poles. This is because at late times (high albedos) the heated hohlraum wall provides the dominant contribution to the drive. As a result of the two LEH's on the poles being spaced farther from other LEH's than the five equatorial LEH's, the poles of the capsule receive more drive. Conversely, at early times (low albedos), the laser-heated spots provide the dominant contribution to the drive. As a result of these spots being more "clumped" around the equator than the poles [Fig. 3(a)], the equatorial region of the capsule receives slightly more drive (but the nonuniformity is still small at 1.1% rms).

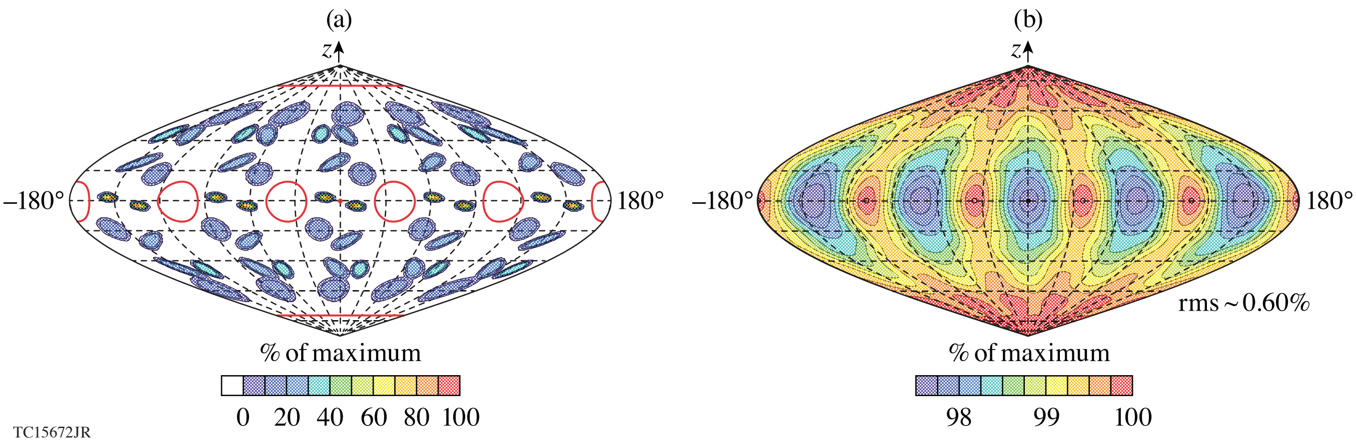

Figure 3
(a) Contour plot of deposited laser energy per unit area on the wall of the PEPR hohlraum. The LEH's are indicated in red. (b) Contour plot of radiation flux variations on the capsule for an albedo of 0.85.

The design was optimized to provide good uniformity at all albedos, i.e., good time-dependent uniformity. This was accomplished by adjusting the aim points of the beams within their LEH's to shift the laser-heated spots closer to the poles. Figure 4(a) shows the dependence of the nonuniformity on albedo for the optimized case, varying from 1.1% at low albedo to 0.6% at high albedo. To achieve this level of time-dependent uniformity requires that both contributions to the drive (laser spots and wall) produce good uniformity since they each dominate at a different time. This is hard to accomplish with cylindrical hohlraums, for which "beam phasing" (different pulse shapes in different sets of beams[2]) is typically required to provide the best balance between the two contributions. While this can produce a low time-averaged nonuniformity, time-dependent nonuniformity can limit the attainable fuel convergence. In the PEPR hohlraum, as in tetrahedral and octahedral hohlraums, all beams can be given the same laser temporal pulse shape.

Figure 4(a) includes, for comparison, an unoptimized PEPR hohlraum design, in which all beams are aimed through the centers of the LEH's. The 6% nonuniformity at low albedo results from the beam spots clumping closer to the equator than shown in Fig. 3(a). The nonuniformity declines at higher albedo as the wall contribution increases. Also shown in Fig. 4(a) is a prediction for optimized tetrahedral hohlraums with the same dimensions. At values of albedo below 0.5, the tetrahedral hohlraum provides better uniformity than the optimized PEPR hohlraum because the locations of deposited laser energy on the tetrahedral hohlraum are more evenly spread out. At albedos greater than 0.5, however, the nonuniformity is lower for the PEPR hohlraum.

A critical role in hohlraum design is played by the case-to-capsule ratio, i.e., the hohlraum radius divided by the capsule radius. It has long been recognized that a large ratio provides better uniformity at the expense of a lower radiation temperature.[2] This

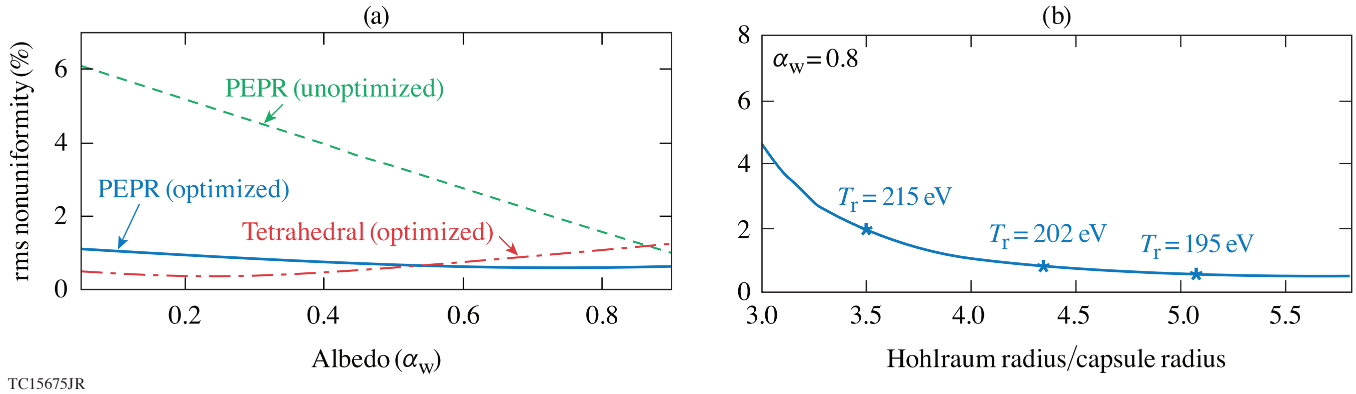

Figure 4
(a) The rms nonuniformity on the capsule for optimized and unoptimized PEPR hohlraums and an optimized tetrahedral hohlraum as a function of albedo. (b) The rms nonuniformity as a function of the ratio of hohlraum radius to capsule radius for the optimized PEPR hohlraum (with the capsule and LEH radii held fixed), illustrating the tradeoff between uniformity and radiation temperature. The albedo here is 0.8.

tradeoff is shown in Fig. 4(b) for the PEPR hohlraum, where the hohlraum radius is varied with the capsule and LEH radii held fixed. The point at a ratio of 5.09 corresponds to the design used in this article, with T_r = 195 eV. This can be increased to 215 eV at a ratio of 3.5 at the expense of a greater nonuniformity of 2%. These values of T_r are limited by the 18-TW laser power assumed here (approximately the peak power used for the OMEGA tetrahedral hohlraum experiments). A NIF-scale PEPR design predicts T_r = 293 eV at a ratio of 3.5 with a nonuniformity of 1.23% (Ref. 14).

An ignition-scale laser system irradiating an octahedral hohlraum would have lower nonuniformity than a PEPR hohlraum for a given case-to-capsule ratio because of the better geometrical symmetry. It would also benefit from more-favorable beam paths because of the elimination of small angles of incidence. While not a candidate for an ignition system, the PEPR hohlraum has the advantage that it can be used on an existing facility, offering a platform for the performance of a variety of experiments. It can be used to demonstrate high-quality spherical implosions using minimal tuning compared with the NIF. Beam phasing is not required: all beams use the same temporal pulse shape. The ratio of hohlraum-to-capsule radius may be adjusted to explore the trade-off between capsule uniformity and background radiation temperature. In addition, the anticipated ease with which near-symmetric implosions can be generated offers a platform for the examination of hot-spot physics and the development of improved diagnostics.

While the PEPR hohlraum promises to drive implosions that are substantially symmetric and 1-D, the geometry is inherently 3-D, requiring 3-D simulations for detailed hohlraum design. Many years ago, the difficulty of carrying out 3-D simulations may have favored the selection of cylindrical hohlraums, which, in spite of their uniformity issues, are well suited to 2-D modeling. The PEPR platform on OMEGA can provide a useful test bed for 3-D modeling.

Further information on this work can be found in Ref. 14.

This material is based upon work supported by the Department of Energy National Nuclear Security Administration under Award Number DE-NA0003856, the University of Rochester, and the New York State Energy Research and Development Authority.

1. J. Nuckolls *et al.*, Nature **239**, 139 (1972).
2. J. D. Lindl, Phys. Plasmas **2**, 3933 (1995).
3. R. S. Craxton *et al.*, Phys. Plasmas **22**, 110501 (2015).
4. C. A. Haynam *et al.*, Appl. Opt. **46**, 3276 (2007).
5. K. Lan *et al.*, Phys. Plasmas **21**, 052704 (2014).

6. K. Lan and W. Zheng, Phys. Plasmas **21**, 090704 (2014).
7. K. Lan *et al.*, Phys. Plasmas **21**, 010704 (2014).
8. D. W. Phillion and S. M. Pollaine, Phys. Plasmas **1**, 2963 (1994).
9. J. D. Schnittman and R. S. Craxton, Phys. Plasmas **3**, 3786 (1996).
10. J. D. Schnittman and R. S. Craxton, Phys. Plasmas **7**, 2964 (2000).
11. J. M. Wallace *et al.*, Phys. Rev. Lett. **82**, 3807 (1999).
12. G. R. Bennett *et al.*, Phys. Plasmas **7**, 2594 (2000).
13. W. A. Farmer *et al.*, Phys. Plasmas **26**, 032701 (2019).
14. W. Y. Wang and R. S. Craxton, Phys. Plasmas **28**, 062703 (2021).